Type of Revision: revision 2
Word count: 5451

Nitrogen diffusion in silicate melts under reducing conditions

Julien Boulliung*, Célia Dalou, Laurent Tissandier, Evelyn Füri, and Yves Marrocchi

Université de Lorraine, CNRS, CRPG, F-54000 Nancy, France

* Corresponding author e-mail address: julienb@crpg.cnrs-nancy.fr

Abstract

The behavior of nitrogen during magmatic degassing and the potential kinetic fractionation between N and other volatile species (H, C, O, noble gases) are poorly known due to the paucity of N diffusion data in silicate melts. To better constrain N mobility during magmatic processes, we investigated N diffusion in silicate melts under reducing conditions. We developed uniaxial diffusion experiments at 1 atm, 1425 °C, and under nominally anhydrous reducing conditions ($fO_2 \leq$ IW –5.1, where IW is oxygen fugacity, fO_2, reported in log units relative to the iron-wüstite buffer), in which N was chemically dissolved in silicate melts as nitride (N^{3-}). Although several experimental designs were tested (platinum, amorphous graphite, and compacted graphite crucibles), only N diffusion experiments at IW – 8 in compacted graphite crucibles for simplified basaltic andesite melts were successful. Measured N diffusivity (D_N) is on the order of $5.3 \pm 1.5 \times 10^{-8}$ cm^2 s^{-1}, two orders of magnitude lower than N chemical diffusion in soda-lime silicate melts (Frischat et al., 1978). This difference suggests that nitride diffusivity increases with increasing degree of melt depolymerization. The dependence of N^{3-} diffusion on melt composition is greater than that of Ar. Furthermore, N^{3-} diffusion in basaltic-andesitic melts is significantly slower than that of Ar in similarly polymerized andesitic-tholeiitic melts at magmatic temperatures (1400–1450 °C; Nowak et al., 2004). This implies that N/Ar ratios can be fractionated during reducing magmatic processes, such as during early-Earth's magma ocean stages.

Keywords: Nitrogen, diffusion, nitride, silicate melts, basaltic andesite.

1. Introduction

Understanding the behavior of volatile elements (H, C, N, noble gases) in silicate melts is fundamental to better constrain their fate during the formation and evolution of Earth and other planetary bodies in the inner solar system (Marty et al., 2016; Piani et al., 2020). Because N, as molecular N_2, is expected to behave like noble gases, particularly Ar, during magmatic processes (Marty, 1995; Miyazaki et al., 1995, 2004), the $N_2/^{36}Ar$ ratios of Earth's atmosphere and mantle are expected to be comparable. However, the $N_2/^{36}Ar$ value of Earth's mantle ($>10^6$, estimated from mid-ocean-ridge basalt glasses) is two orders of magnitude higher than that of the atmosphere ($\sim10^4$) (Marty, 1995; Marty et al., 1995; Marty and Humbert, 1997), perhaps as a result of kinetic disequilibrium during the formation of Earth's atmosphere due to mantle degassing (Marty et al., 1995) or the distinct volatile histories of these two reservoirs (Marty and Humbert, 1997). Diffusion strongly controls this ratio because it governs volatile transport and degassing during magmatic activity at all stages of planetary evolution (from magma ocean differentiation to volcanic eruptions). However, whereas the diffusion of H_2O, CO_2, and noble gases in silicate melts has been widely studied (e.g., Zhang and Stolper, 1991; Baker et al., 2005; Zhang and Ni, 2010; Lux, 1987; Roselieb et al., 1995; Amalberti et al., 2018), N diffusion in silicate melts remains largely under-constrained.

Elemental speciation fundamentally controls the diffusion of redox-sensitive species such as nitrogen in silicate melts (Frischat et al., 1978; Zhang and Ni, 2010). Depending on fO_2 conditions, N is incorporated as free molecular N_2 and NH_3 or bonded N^{3-}, CN^-, NH^{2-}, and/or NH_2^- (Libourel et al., 2003; Li et al., 2015; Dalou et al., 2017, 2019; Mosenfelder et

al., 2019; Boulliung et al., 2020; Grewal et al., 2020). At atmospheric pressure and under anhydrous conditions, N is either incorporated as molecular N_2 under oxidizing conditions (fO_2 > IW –1.5) or chemically dissolved as nitride (N^{3-}) under reducing conditions ($fO_2 \leq$ IW –1.5; Libourel et al., 2003; Boulliung et al., 2020). To date, N diffusion in silicate melts has only been studied in soda-lime silicate melts at atmospheric pressure and high temperature (1000–1400 °C) for molecular N_2 and nitride species (Frischat et al., 1978). In these melts, physical diffusion of N_2 is significantly faster than chemical diffusion of nitride (Behrens, 2010). However, N solubility not only depends on fO_2, but also on melt composition and structure; when dissolved as N^{3-}, N solubility increases with increasing degree of melt depolymerization (Boulliung et al., 2020). These observations indicate that melt composition may affect N diffusion, and, therefore, that N diffusivities determined for soda-lime silicate melts cannot be representative of those in natural silicate melts.

In this study, various experimental approaches were tested to determine uniaxial N diffusion in silicate melts of simplified basaltic andesite and highly depolymerized, magma ocean-like compositions to address the influence of melt composition on N diffusion under conditions in which N is chemically incorporated as nitride. Uniaxial diffusion experiments were conducted at 1425 °C, 1 atm, and IW –8 and IW –5.1. Nitrogen concentration profiles in the quenched run products were determined by *in-situ* secondary ion mass spectrometry (SIMS). The results provide new insights into the N diffusion mechanism(s) in naturally occurring silicate melts, thereby improving our understanding of the behavior of N during reducing magmatic processes.

2. Experimental and analytical methods

Two starting materials of different simplified iron-free compositions were synthesized and their bulk compositions determined by electron microprobe analysis at Université de

Lorraine (Service Commun de Microscopie Electronique et de Microanalyses X, Nancy, France): (i) a basaltic andesite composition (AND1; 53.6 wt% SiO_2, 20.7 wt% Al_2O_3, 9.9 wt% MgO, 15.0 wt% CaO, 0.45 wt% Na_2O, 0.16 wt% K_2O) and (ii) a mafic composition (MO2; 47.4 wt% SiO_2, 4.6 wt% Al_2O_3, 19.8 wt% MgO, 26.1 wt% CaO). These starting glass materials are characterized by extreme NBO/T values (the number of non-bridging oxygen atoms per tetrahedrally coordinated cations) of 0.5 (AND1) and 2.1 (MO2); the latter is comparable to that estimated for the terrestrial magma ocean (Ringwood, 1966; Dasgupta and Grewal, 2019). To prepare these starting materials, oxide and carbonate powders were dried and decarbonated at 1000 ºC in a muffle furnace for 12 h. After mixing in appropriate proportions, they were fused in a platinum crucible at 1400 °C in a muffle furnace for 4 h and quenched in air. The fused starting glasses AND1 and MO2 were ground for 1 h for use in the different experiments.

Different experimental supports were tested to study uniaxial N diffusion. Compacted graphite (15 mm long, 6 mm outer diameter, 1.5 mm wall thickness) and vitreous graphite (12 mm long, 7 mm outer diameter, 1 mm wall thickness) cylinders were used for experiments at IW –8, whereas Pt cylinders (13 mm long, 3 mm outer diameter, 0.2 mm wall thickness) were used for experiments at IW –5.1 (Table 1). To obtain bubble-free glass prior to the diffusion experiments, the starting powder was incrementally filled into the cylinders and melted for 30 min under a CO_2 flux (300 cm^3 min^{-1}) at 1600 °C for Pt crucibles (as described by Amalberti et al., 2018) and under Ar flux (300 cm^3 min^{-1}) at 1450 °C for graphite cylinders to minimize potential atmospheric nitrogen contamination. The filled cylinders were subjected to a final melting step at 1550 °C for Pt crucibles and 1450 °C for graphite crucibles during ~15 h under the same Ar and CO_2 fluxes to ensure the complete removal of bubbles.

Uniaxial N diffusion experiments were performed in a Gero vertical furnace at atmospheric pressure, 1425 ± 1 °C, and under a controlled N_2-CO(-CO_2) atmosphere at log

fO_2 = –17.4 and –14.5 (IW –8 and IW –5.1, respectively; Table 1). Diffusion at such low oxygen fugacities is expected to result in discernable and measurable N concentration gradients, whereas low N solubilities in silicate melts under more oxidizing conditions (log fO_2 > IW –1.5) limit N contents to a few ppm (Libourel et al., 2003; Boulliung et al., 2020). The gas flux was maintained at 300 cm^3 min^{-1} by TYLAN mass flow controllers. The graphite cylinders were placed into an alumina crucible, whereas the platinum cylinders were held in place using Pt wire (0.3 mm). Diffusion experiments using compacted graphite and vitreous graphite cylinders lasted 3 h, but were restricted to 1 h with Pt crucibles to minimize Pt loss by evaporation at high temperature under reducing conditions (Darling et al., 1970) (Table 1). Regardless of melt composition, these experimental durations are too short to reach gas-melt equilibrium; based on experiments using 2–5 mm diameter silicate melt spherules in graphite crucibles, equilibrium is expected to be achieved in 24 hours (Humbert, 1998; Boulliung et al., 2020). After quenching in air, run products were fixed onto a flat ceramic support using Crystalbond™ adhesive and cut in half along the direction of diffusion. The obtained glass half-cylinders were then mounted in high-purity indium, polished, and gold coated.

N concentrations were quantified by *in-situ* measurements of $^{14}N^{16}O^-$ secondary ions using the CAMECA 1280 HR2 SIMS at the Centre de Recherches Pétrographiques et Géochimiques (Nancy, France) operating with a 10 kV Cs^+ primary ion beam, a current of ~10 nA, and a nominal mass resolution of ~13,000 (for details, see Füri et al., 2018). N contents were measured along profiles from each exterior edge of the glass cylinders towards their center (Fig. 1). Uncertainties on N contents (2σ) are ≤4% for N contents >100 ppm, ≤30% between 10 and 100 ppm, and 50–100% below 10 ppm. Carbon (CO_2) and water (H_2O) contents were measured in one sample (along profile A of AND1; Fig. 1) using the CAMECA

IMS-1270 E7 ion microprobe (see supplementary material for details) to assess the potential presence and abundance of these volatiles.

Results

Previous gas-melt equilibrium experiments at IW –5.1 yielded N contents of 68.1 ± 6.0 ppm and 35.6 ± 10.7 ppm for AND1 and MO2, respectively, and those at IW –8 yielded 2672 ± 40 ppm and 5987 ± 63 ppm, respectively, after 24 hours (Boulliung et al., 2020). These experiments demonstrated that N solubility is highest in depolymerized melts under very reducing conditions.

The run products of diffusion experiments performed with platinum crucibles at IW –5.1 contain <5 ppm N, and concentrations are indistinguishable within analytical uncertainties. The glasses produced using vitreous graphite crucibles at IW –8 have homogeneous N concentrations (208 ± 10 ppm in AND1 and 400 ± 47 ppm in MO2) and lack any apparent diffusion profiles. Therefore, N diffusion coefficients could not be determined in experiments using platinum and vitreous graphite crucibles.

A significant loss of melt (~50%) and partial crystallization was observed in the experiment on the MO2 melt using a compacted graphite crucible at IW –8. Given its high degree of depolymerization (NBO/T = 2.1) and correspondingly low viscosity, this melt loss was likely caused by melt migration. We assume that minor evaporation of major oxides (mainly SiO_2 and MgO) during the bubble elimination steps (at 1450°C under an Ar flux), affected the liquidus temperature (initially estimated just below ~1400°C) and promoted crystallization upon quenching. Due to these limitations, no nitrogen diffusion profiles were observed for the MO2 melt. In contrast, using the same experimental design, the AND1 melt was successfully quenched to a crystal-free glass, and N concentration gradients were determined along four profiles (A–D; Fig. 1). The N concentrations range from 1068 ± 41 to 4

± 3 ppm, 142 ± 5 to 7 ± 4 ppm, 220 ± 9 to 8 ± 4 ppm, and 2001 ± 80 to 541 ± 22 ppm along profiles A, B, C, and D, respectively (Fig. 1, Table 2). Although the surface of the melt adopts the shape of a concave meniscus (Fig. 1E), N concentrations along the gas-melt interface are nearly homogeneous (906 ± 37 to 1068 ± 41 ppm; supplementary Fig. A1).

Discussion

The N contents of glasses produced in experiments using Pt crucibles are too low (<5 ppm) to detect concentration gradients by SIMS. Although the 1-h experimental duration was probably too short to dissolve a significant amount of N, even at low fO_2 conditions (IW –5.1) under which N contents are expected to be relatively important at gas-melt equilibrium (i.e., tens of ppm; Boulliung et al., 2020), longer experiments were not possible because Pt crucibles are prone to evaporative losses at such strongly reducing conditions. The run products of experiments using vitreous graphite are N-rich (208 ± 10 ppm in AND1, 400 ± 47 ppm in MO2), but were likely homogenized by convection induced by the bottom-up migration of silicate melts along the vitreous graphite crucible. We therefore conclude that platinum and vitreous graphite are not appropriate for experiments on N diffusion in silicate melt under reducing conditions.

On the other hand, the uniaxial diffusion experiment using compacted graphite yielded variable N concentration gradients in glass AND1 (Fig. 1). The occurrence of N gradients along profiles B, C, and D (Fig. 1) is surprising since no direct gas-melt interaction was expected at the edges or bottom of the glass cylinder. These gradients may be the result of N migration along or diffusion through the graphite crucible. Nevertheless, the central part of the glass cylinder is N-free (Table 2) which suggests that no or very limited convection movements occurred in the melt during the experiment. The N diffusion coefficients can be

180 determined from each profile using the one-dimensional diffusion equation in a semi-infinite
181 medium with a constant interface concentration (Crank, 1975):

182 $$\frac{(C(x,t)-C_1)}{(C_0-C_1)} = \mathrm{erf}\left(\frac{x}{2\sqrt{Dt}}\right) \quad (1)$$

183
184 where $C(x,t)$ is the concentration at distance x from the gas-melt interface after time t (the
185 experimental duration), C_0 is the initial concentration in the glass (here, $C_0 = 0$), C_1 is the
186 concentration at the gas-melt interface ($x = 0$), and D is the diffusion coefficient. For profile
187 A, we chose the starting point ($x = 0$) to be at the center of the meniscus, whereas the starting
188 point for the other profiles was chosen arbitrarily. In each case, the concentration at the gas-
189 melt interface was obtained by extrapolating the diffusion profile to $x = 0$. Finally, we
190 linearized the left-hand side of equation (1) by plotting the inverse error function against
191 distance to extract the diffusion coefficient as (Van Orman et al., 1998):

192 $$D = (4m^2t)^{-1} \quad (2)$$

193 The slope of the best-fit line, m, was derived using IsoplotR (Vermeech 2018) with an
194 uncertainty that takes into account the uncertainties on measured N concentrations and on x
195 positions (5 µm). The diffusion coefficients are reported in Figure 1, and the inversion error
196 function of diffusion profile A is presented as a representative example in Figure 2. Because
197 of the meniscus shape of the gas-melt interface (Fig. 1E), N diffusion may not be strictly one-
198 dimensional along profile A. Thus, the main source of uncertainty for profile A is related to
199 the position of the origin of the diffusion profile ($x = 0$). The overall uncertainty was
200 evaluated by comparing the diffusion coefficient for a starting point at the center ($4.2 \pm 0.4 \times$
201 10^{-8} cm^2 s^{-1}) and at mid-height of the meniscus ($6.2 \pm 0.6 \times 10^{-8}$ cm^2 s^{-1}). By coupling the
202 standard deviation related to the geometrical and the analytical uncertainties, the average
203 diffusion coefficient is equal to $5.3 \pm 1.5 \times 10^{-8}$ cm^2 s^{-1} along profile A. The diffusion
204 coefficients obtained for the four profiles differ significantly, with lower values for profiles B,
205 C and D (Fig. 1), likely due to distinct boundary conditions; given that N diffusion along

profiles B, C, and D may have been controlled by delayed transport of nitrogen through the graphite container wall, these three values are excluded from further discussions.

To date, the diffusion of molecularly (N_2) and chemically incorporated nitrogen (N^{3-}) in silicate melts has only been studied in soda-lime silicate compositions at atmospheric pressure and 1000–1400 °C (Frischat et al., 1978). The authors studied N_2 diffusion by heating a pre-saturated glass slab under an oxygen atmosphere and chemical diffusion by heating a glass containing silicon nitride under an Ar-H_2 atmosphere. Under these conditions, N diffuses faster as N_2 than N^{3-} in soda-lime silicate melts (Frischat et al., 1978; Behrens, 2010). However, nitride diffusivity increases more rapidly than N_2 diffusivity with increasing temperature because of its higher activation energy (244 kJ mol^{-1} for N^{3-} *vs.* 161 kJ mol^{-1} for N_2; Frischat et al., 1978). Indeed, N_2 displays an intrinsic diffusivity resembling that of noble gases (Dingwell and Webb, 1990; Dingwell, 2006), whereas N^{3-} diffusivity seems to be extrinsic, as it increases significantly with increasing temperature.

Under nominally anhydrous and very reducing conditions (i.e., IW –8), N is expected to dissolve predominantly as nitride species (Libourel et al., 2003), likely bonded as Si-N (Boulliung et al., 2020), whereas C-N and N-H species are inferred to represent a minor fraction of the total N budget (see supplementary material for details). After extrapolation of the data from Frischat et al. (1978) to 1425 °C, N^{3-} diffusion in soda-lime silicate melts is two orders of magnitude higher (~6.0×10^{-6} cm^2 s^{-1}) than in our melt AND1 ($5.3 \pm 1.5 \times 10^{-8}$ cm^2 s^{-1}). As soda-lime silicate melts are more depolymerized (NBO/T = 0.7) than basaltic andesite melts (NBO/T = 0.5), it appears that N^{3-} diffusion increases with melt depolymerization. However, since the experimental conditions (e.g., fO_2) of the study of Frischat et al. (1978) are not clearly indicated, it is difficult to ascertain that the NBO/T value is the only parameter responsible for this difference. Although additional experiments, including distinct melt compositions, are needed to better understand the effect of melt polymerization on N^{3-}

231 diffusion, we note here that similar behavior is observed for O^{2-}, for which the activation
232 energy decreases with increasing depolymerization (e.g., Lesher, 2010). As in the case of
233 oxygen, nitride diffusion requires the breaking of Si-O bonds, and the increased occurrence of
234 Si-O-M (where M is a network-modifying cation and O a non-bridging oxygen) compared to
235 Si-O-Si bounds (with O a bridging oxygen) in highly depolymerized melts enhances nitride
236 diffusion by oxygen substitution (Boulliung et al., 2020). To compare the diffusivity of
237 network formers (such as Si and Al) and O^{2-} (e.g., Dingwell and Webb, 1990) with that of
238 nitride obtained for profile A, we used the Eyring equation:

239 $$D = \frac{kT}{\eta\lambda} \qquad (3)$$

240 where D is the diffusion coefficient in $m^2\ s^{-1}$; k is the Boltzmann constant, T is the
241 temperature in K, η is the melt viscosity in Pa s, and λ is the jump distance, which is fixed at 3
242 Å for the diffusion of network formers (e.g., Nowak et al., 2004). The melt viscosity (η) of
243 AND1 at 1425°C is 2.19 P as (calculated using the model of Giordano et al., 2008) (see
244 supplementary material for details). The Eyring diffusivity at 1425°C, ~3.6×10^{-7} $cm^2\ s^{-1}$, is
245 less than one order of magnitude higher than the diffusion coefficient obtained for N in this
246 study ($5.3 \pm 1.5 \times 10^{-8}$ $cm^2\ s^{-1}$; supplementary Fig. A2). This similarity suggests that
247 movements of network formers are involved in nitride diffusion, reinforcing the conclusion of
248 Boulliung et al. (2020) that N diffuses as a Si-N species under highly reducing conditions in
249 basaltic andesite melts.

250 As with N^{3-} and O^{2-}, noble gas diffusivity also increases with increasing degree of melt
251 depolymerization. For example, at 1400 °C, Amalberti et al. (2018) reported that the argon
252 diffusion coefficient (D_{Ar}) in a synthetic basaltic melt with NBO/T = 1 (9.3×10^{-7} $cm^2\ s^{-1}$) is
253 ~3 times higher than that in a synthetic Hawaiitic melt with NBO/T = 0.7 (2.9×10^{-7} $cm^2\ s^{-1}$;
254 Nowak et al. 2004). The relative difference in NBO/T between the soda-lime silicate melt
255 (NBO/T = 0.7) used by Frischat et al. (1978) and our melt AND1 (NBO/T = 0.5) is

256 comparable to that between basaltic and Hawaiitic melts. However, D_N is ~110 times higher
257 in soda-lime silicate melts than in AND1, indicating that nitride diffusion is more dependent
258 on the degree of melt polymerization than Ar diffusion in this temperature range.
259 Furthermore, at the same degree of melt polymerization (NBO/T = 0.5), $D_{Ar} = 1.5 \times 10^{-7}$ cm^2
260 s^{-1} in andesitic-tholeiitic melts at 1400–1450 °C and 500 MPa (Nowak et al., 2004), is ~3
261 times higher than the D_N value observed for our AND1 melt (5.3×10^{-8} cm^2 s^{-1}). Since
262 increased pressure slows down noble gas diffusion in silicate melts (Roselieb et al., 1996;
263 Behrens and Zhang, 2001; Zhang et al., 2007), D_{Ar} is expected to be even larger at 1 atm. This
264 difference between D_{Ar} and D_N suggests that under reducing conditions (i.e., N as N^{3-}),
265 diffusion during magmatic processes significantly fractionates the N/Ar ratio.
266
267 **Implications**
268 Our results imply the efficient transport of N as nitride under magma ocean conditions
269 during early stages of Earth's formation (i.e., fO_2 between IW –3 and IW –5 for 70% of
270 Earth's mass accreted, Rubie et al., 2011; Wade and Wood, 2005; ~2000 K, Rubie, 2007;
271 Solomatov, 2007; and NBO/T ~ 2, Ringwood, 1966; Javoy et al., 2010; Dasgupta and Grewal,
272 2019). Under such conditions favorable to nitrogen diffusion as nitride, the N/Ar ratio may be
273 kinetically fractionated during degassing and/or ingassing and melt migration. Therefore, the
274 different N/Ar ratios of Earth's mantle and atmosphere (e.g., Marty, 1995) may have resulted
275 from an early stage of atmospheric formation when Earth's magma ocean was highly
276 reducing. During later stages of magma ocean differentiation, for redox conditions between
277 IW –3 and IW –1.5 (i.e., when Earth had accreted more than 70% of its final mass, Rubie et
278 al., 2011), N dissolves not only as N^{3-}, but as other species such as N-H or C-N complexes,
279 and, to a lesser extent, N_2 (e.g., Dalou et al., 2019; Grewal et al., 2020; Boulliung et al. 2020)
280 depending on fH_2 and fO_2. Since the speciation of volatile elements affects their diffusivity in

silicate melts (e.g., Frischat et al., 1978; Zhang and Ni, 2010), the diffusion and transport mechanism(s) of such species needs to be investigated through multi-component experiments over a range of P-T-fO_2 conditions. With this respect, the experimental design (gas-melt interaction in compacted graphite crucibles), analytical protocol (*in situ* SIMS analysis), and first results presented here represent an important step towards improving our understanding of N behavior within planetary magma oceans.

Figure captions

Fig. 1. Nitrogen concentration profiles A–D measured in glass cylinder AND1 (1 atm, 1425 °C, 3 h, IW –8); the respective SIMS spot analyses are the small dark spots in the photograph in panel E. The indicated equilibrium nitrogen concentration (2672 ± 40 ppm) is that determined from the 24-h gas-melt equilibrium experiment on AND1 under similar experimental conditions (Boulliung et al., 2020). The diffusion coefficient (and the uncertainty thereof) along profile A takes into account the geometrical and analytical uncertainties (see text for details).

Fig. 2. Error function inversion of profile A (Fig. 1) as a function of depth in the sample (for x = 0, i.e., a starting point at the center of the meniscus). The nitrogen diffusion coefficient D_N was calculated using the inverse error function according to equations (1) and (2). The linear regression between the inverse function of concentration and depth was calculated using IsoplotR (Vermeesch, 2018).

This is the peer-reviewed, final accepted version for American Mineralogist, published by the Mineralogical Society of America.
The published version is subject to change. Cite as Authors (Year) Title. American Mineralogist, in press.
DOI: https://doi.org/10.2138/am-2021-7799CCBYNCND. http://www.minsocam.org/

Figure 1

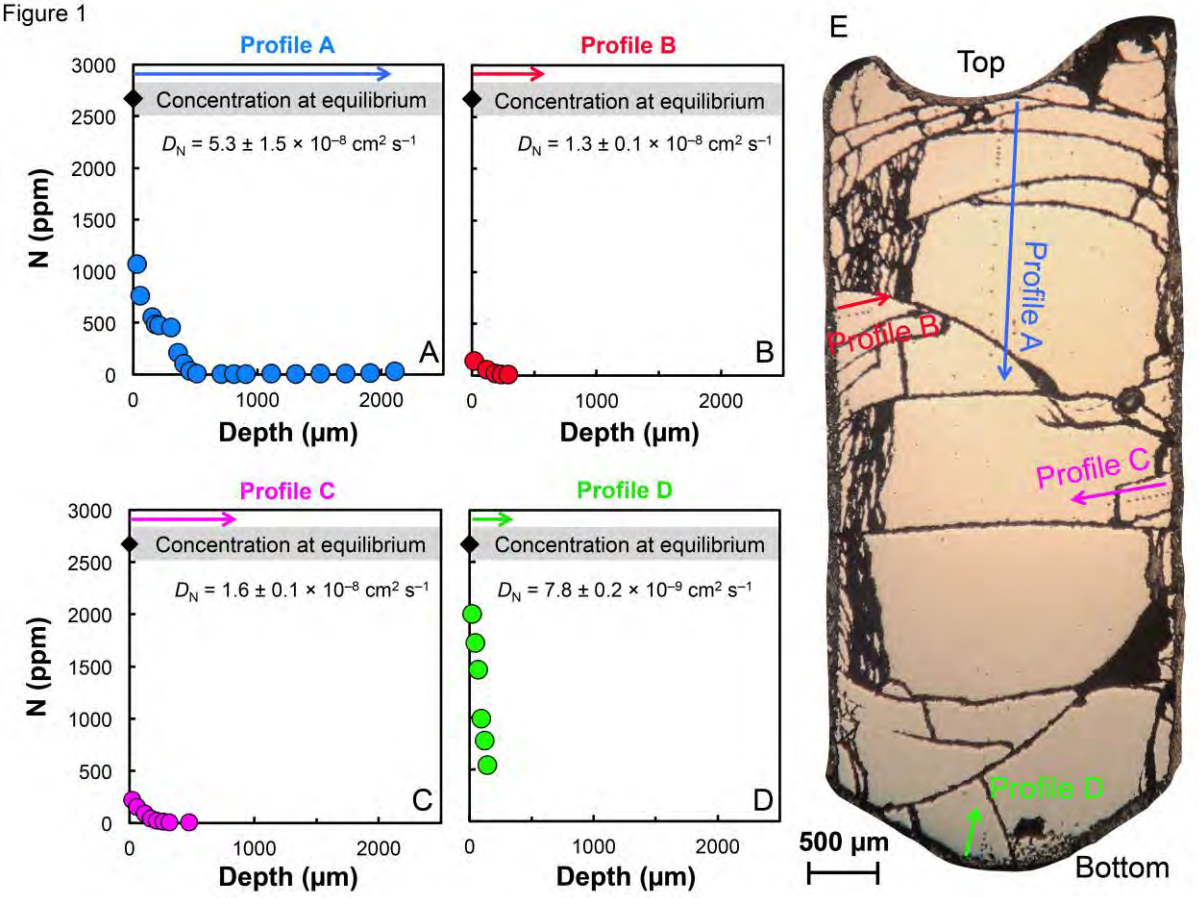

304

305

Figure 2

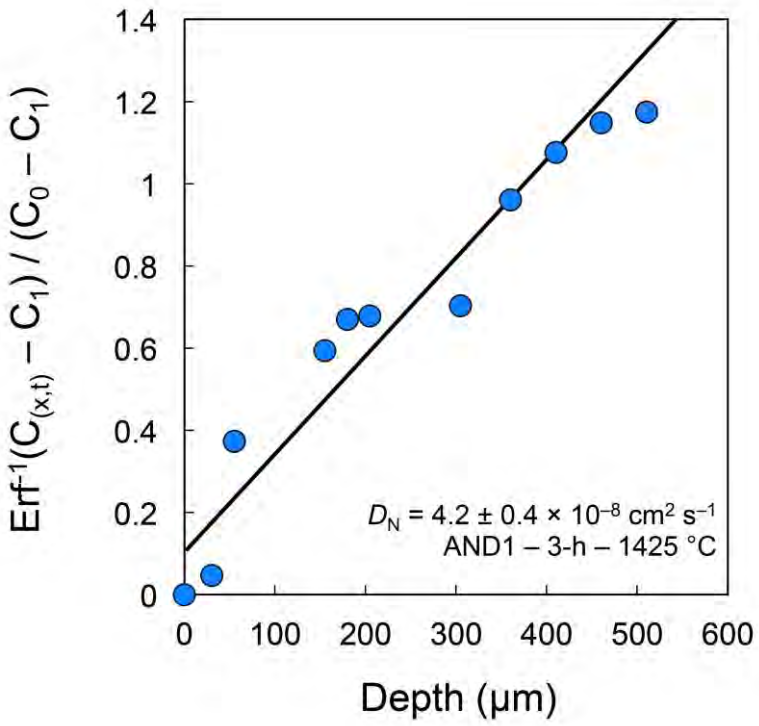

Table 1. Run conditions and fractional gas mixtures of nitrogen nominally uniaxial diffusion (1–3 h) at P = 1 atm, T = 1425 °C for both AND1 and MO2 melt compositions. These nominal fO_2 values were calculated using the JANAF and Thermodata database (see Boulliung et al., 2020, for details).

fO_2 (IW)	log fO_2	Sample holder	Duration (hours)	CO	CO_2	N_2
IW –8	–17.4	Vitreous graphite	3	0.2	–	0.8
IW –8	–17.4	Compacted graphite	3	0.2	–	0.8
IW –5.1	–14.5	Platinum	1	0.4994	0.0006	0.5

Table 2: N contents measured along the profiles presented in Figure 1A–D. SIMS spot references refer to the profile (A–D) and number of each analysis along the profile as indicated by the arrows in Figure 1E.

SIMS spot reference	Depth (µm)	N (ppm)
A-1	30	1068 ± 41
A-2	55	762 ± 15
A-3	155	556 ± 11
A-4	180	485 ± 10
A-5	205	477 ± 10
A-6	305	454 ± 9
A-7	360	212 ± 5
A-8	410	104 ± 4
A-9	460	36 ± 5
A-10	510	11 ± 3
A-11	710	4 ± 3
A-12	810	5 ± 3
A-13	910	6 ± 4
A-14	1110	7 ± 4
A-15	1310	6 ± 4
A-16	1510	7 ± 4
A-17	1710	9 ± 4
A-18	1910	15 ± 3
A-19	2110	33 ± 3
B-1	20	142 ± 5
B-2	120	56 ± 4
B-3	190	22 ± 3
B-4	240	10 ± 5
B-5	290	7 ± 4
C-1	20	220 ± 9
C-2	60	156 ± 6
C-3	120	89 ± 9
C-4	170	41 ± 6
C-5	220	20 ± 6
C-6	270	13 ± 4
C-7	320	10 ± 5
C-8	480	8 ± 4
D-1	20	2001 ± 80
D-2	45	1720 ± 69
D-3	70	1460 ± 58
D-4	95	993 ± 40
D-5	120	777± 31
D-6	145	541 ± 22

Acknowledgments

Delphine Lequin is thanked for her help during the diffusion experiments. Technical support by Cécile Deligny, Etienne Deloule, Nordine Bouden, and Johan Villeneuve (SIMS), and Olivier Rouer (electron microprobe), is gratefully acknowledged, and we thank François Faure for constructive discussions. Robert Dennen is thanked for English editing. Constructive comments by associate editor Charles E. Lesher, Harald Behrens, and an anonymous reviewer helped to improve the manuscript. This work was supported by the European Research Council (ERC) under the European Union's Horizon 2020 research and innovation program (grant agreement no. 715028). This is CRPG contribution 2733.

References

Amalberti, J., Burnard, P., Tissandier, L., and Laporte, D. (2018) The diffusion coefficients of noble gases (He–Ar) in a synthetic basaltic liquid: One-dimensional diffusion experiments. Chemical Geology, 480, 35–43.

Baker, D.R., Freda, C., Brooker, R.A., and Scarlato, P. (2005) Volatile diffusion in silicate melts and its effects on melt inclusions. Annals of Geophysics, 48(4–5), 699–717.

Behrens, H. (2010) Noble gas diffusion in silicate glasses and melts. Reviews in Mineralogy and Geochemistry, 72(1), 227-267.

Behrens, H., and Zhang, Y. (2001) Ar diffusion in hydrous silicic melts: implications for volatile diffusion mechanisms and fractionation. Earth and Planetary Science Letters, 192(3), 363–376.

Boulliung, J., Füri, E., Dalou, C., Tissandier, L., Zimmermann, L., and Marrocchi, Y (2020) Oxygen fugacity and melt composition controls on nitrogen solubility in silicate melts. Geochimica et Cosmochimica Acta, 284, 120-133.

Crank, J. (1975) The mathematics of diffusion 2nd Edition. Oxford Science Publications, 32.

Dalou, C., Hirschmann, M.M., von der Handt, A., Mosenfelder, J., and Armstrong, L.S. (2017) Nitrogen and carbon fractionation during core–mantle differentiation at shallow depth. Earth and Planetary Science Letters, 458, 141–151.

Dalou, C., Hirschmann, M.M., Jacobsen, S.D., and Le Losq, C. (2019) Raman spectroscopy study of COHN speciation in reduced basaltic glasses: Implications for reduced planetary mantles. Geochimica et Cosmochimica Acta 265, 32–47.

Darling, A.S., Selman, G.L., and Rushforth, R. (1970) Platinum and the refractory oxides. I. Compatibility and decomposition processes at high temperatures. Johnson Matthey and Co., Ltd., London.

Dasgupta, R., and Grewal, D.S. (2019) Origin and Early Differentiation of Carbon and Associated Life-essential Volatile Elements on Earth. In Deep Carbon (pp. 4–39). Cambridge University Press.

Dingwell, D.B. (2006) Transport properties of magmas: diffusion and rheology. Elements, 2(5), 281–286.

Dingwell, D.B., and Webb, S. L. (1990) Relaxation in silicate melts. European Journal of Mineralogy, (4), 427–449.

Frischat, G.H., Buschmann, O., and Meyer, H. (1978) Diffusion von Sticktoff in Glasschmelzen. Glastechnische Berichte 51, 321–327.

Füri, E., Deloule, E., and Dalou, C. (2018) Nitrogen abundance and isotope analysis of silicate glasses by secondary ionization mass spectrometry. Chemical Geology, 493, 327–337.

Giordano, D., Russell, J.K., and Dingwell, D.B. (2008) Viscosity of magmatic liquids: a model. Earth and Planetary Science Letters, 271(1–4), 123–134.

Grewal, D.S., Dasgupta, R., and Farnell, A. (2020) The speciation of carbon, nitrogen, and water in magma oceans and its effect on volatile partitioning between major reservoirs of the Solar System rocky bodies. Geochimica et Cosmochimica Acta.

Humbert, F. (1998) Solubilité de l'azote dans les silicates liquides influence de la fugacité d'oxygène et de la composition, 234 p. Ph.D. thesis, Université Henri Poincaré-Nancy 1 (in French).

Javoy, M., Kaminski, E., Guyot, F., Andrault, D., Sanloup, C., Moreira, M., Labrosse, S., Jambon, A., Agrinier, P., Davaille, A., and Jaupart, C. (2010) The chemical composition of the Earth: Enstatite chondrite models. Earth and Planetary Science Letters, 293(3–4), 259–268.

Lesher, C.E. (2010) Self-diffusion in silicate melts: theory, observations and applications to magmatic systems. Reviews in Mineralogy and Geochemistry, 72(1), 269–309.

Li, Y., Huang, R., Wiedenbeck, M., and Keppler, H. (2015) Nitrogen distribution between aqueous fluids and silicate melts. Earth and Planetary Science Letters, 411, 218–228.

Libourel, G., Marty, B., and Humbert, F. (2003) Nitrogen solubility in basaltic melt. Part I. Effect of oxygen fugacity. Geochimica et Cosmochimica Acta, 67(21), 4123–4135.

Lux, G. (1987) The behavior of noble gases in silicate liquids: Solution, diffusion, bubbles and surface effects, with applications to natural samples. Geochimica et Cosmochimica Acta, 51(6), 1549–1560.

Marty, B. (1995) Nitrogen content of the mantle inferred from N 2–Ar correlation in oceanic basalts. Nature, 377(6547), 326–329.

Marty, B., Lenoble, M., and Vassard, N. (1995) Nitrogen, helium and argon in basalt: a static mass spectrometry study. Chemical geology, 120(1–2), 183–195.

Marty, B., and Humbert, F. (1997) Nitrogen and argon isotopes in oceanic basalts. Earth and Planetary Science Letters, 152(1–4), 101–112.Marty, B., Lenoble, M., & Vassard, N. (1995). Nitrogen, helium and argon in basalt: a static mass spectrometry study. Chemical geology, 120(1–2), 183–195.

Marty, B., Avice, G., Sano, Y., Altwegg, K., Balsiger, H., Hässig, M., Morbidelli, A., Mousis, O., and Rubin, M. (2016) Origins of volatile elements (H, C, N, noble gases) on Earth and Mars in light of recent results from the ROSETTA cometary mission. Earth and Planetary Science Letters, 441, 91–102.

Miyazaki, A., Hiyagon, H., and Sugiura, N. (1995) Solubilities of nitrogen and argon in basalt melt under oxidizing conditions. In American Institute of Physics Conference Proceedings 341(1), 276–283.

Miyazaki, A., Hiyagon, H., Sugiura, N., Hirose, K., and Takahashi, E. (2004) Solubilities of nitrogen and noble gases in silicate melts under various oxygen fugacities: implications for the origin and degassing history of nitrogen and noble gases in the Earth. Geochimica et Cosmochimica Acta, 68(2), 387–401.

Mosenfelder, J.L., Von Der Handt, A., Füri, E., Dalou, C., Hervig, R.L., Rossman, G.R., and Hirschmann, M.M. (2019) Nitrogen incorporation in silicates and metals: Results from SIMS, EPMA, FTIR, and laser-extraction mass spectrometry. American Mineralogist: Journal of Earth and Planetary Materials, 104(1), 31–46.

Nowak, M., Schreen, D., and Spickenbom, K. (2004) Argon and CO2 on the race track in silicate melts: a tool for the development of a CO2 speciation and diffusion model. Geochimica et Cosmochimica Acta, 68(24), 5127–5138.

Piani, L., Marrocchi, Y., Rigaudier, T., Vacher, L. G., Thomassin, D., & Marty, B. (2020). Earth's water may have been inherited from material similar to enstatite chondrite meteorites. Science, 369(6507), 1110–1113.

Ringwood, A.E. (1966) Chemical evolution of the terrestrial planets. Geochimica et Cosmochimica Acta, 30(1), 41–104.

Roselieb, K., Rammensee, W., Büttner, H., and Rosenhauer, M. (1995) Diffusion of noble gases in melts of the system SiO2 NaAlSi2O6. Chemical Geology, 120(1-2), 1-13.

Roselieb, K., Büttner, H., Eicke, U., Köhler, U., and Rosenhauer, M. (1996) Pressure dependence of Ar and Kr diffusion in a jadeite melt. Chemical geology, 128(1–4), 207–216.

Rubie, D.C. (2007) Formation of Earth's core. Evolution of the Earth, 51–90.

Rubie, D.C., Frost, D. J., Mann, U., Asahara, Y., Nimmo, F., Tsuno, K., Kegler, P., Holzheid, A., and Palme, H. (2011) Heterogeneous accretion, composition and core–mantle differentiation of the Earth. Earth and Planetary Science Letters, 301(1-2), 31–42.

Solomatov, V.S. (2007) Magma oceans and primordial mantle differentiation. Treatise on geophysics, 9, 91–120.

Van Orman, J.A., Grove, T.L., and Shimizu, N. (1998) "Uranium and thorium diffusion in diopside". Earth and Planetary Science Letters (160), 505-519.

Vermeesch, P. (2018) IsoplotR: a free and open toolbox for geochronology. Geoscience Frontiers 9(5), 1479–1493.

Wade, J., and Wood, B. J. (2005) Core formation and the oxidation state of the Earth. Earth and Planetary Science Letters, 236(1-2), 78-95.

Zhang, Y., and Ni, H. (2010) "Diffusion of H, C, and O components in silicate melts". Mineralogy & Geochemistry 72, 171–225.

Zhang, Y., and Stolper, E. M. (1991) Water diffusion in a basaltic melt. Nature, 351(6324), 306-309.

Zhang, Y., Xu, Z., Zhu, M., and Wang, H. (2007) Silicate melt properties and volcanic eruptions. Reviews of Geophysics, 45(4).